*

Novel Templated Mesoporous Carbons as Electrode for Electrochemical Capacitors with Aqueous Neutral Electrolytes

J. Ortiz-Bustos [a], S. G. Real [b], M. Cruz [c], J. Santos-Peña [d,e,*]

[a] Departamento de Tecnología Química y del Medio ambiente, ESCET, Universidad Rey Juan Carlos, 28933 Móstoles (Spain)

[b] Instituto de Investigaciones Fisicoquímicas Teóricas y Aplicadas, Facultad de Ciencias Exactas, Universidad Nacional de La Plata, 1900 La Plata (Argentina)

[c] Departamento de Química Inorgànica e Ingeniería Química, Instituto Universitario de Química Fina y Nanoquímica, Universidad de Córdoba, 14071 Córdoba (Spain)

[d] Laboratoire de Physicochimie des Matériaux et Electrolytes pour l'Energie, Campus de Grandmont, Université de Tours, 37200 Tours (France)

[e] Laboratoire de Recherche Correspondant PCM2E-CEA Le Ripault, 37260 Monts (France)

[*] Corresponding author : jesus.santos-pena@univ-tours.fr

ABSTRACT

In search for new electrodes for electrochemical capacitors, two template mesoporous carbons (TMC) are prepared with the replica method by using Plugged Hexagonal Templated Silica (PHTS) and Mesostructured Cellular Foam (MCF) as hard templates. No subsequent activation after synthesis is carried out in order to correlate textural and electrochemical properties in neutral sulfate electrolytes. TMC show interesting textural and conductive properties for capacitor electrode purposes: specific surface areas higher than 1000 $m^2 \cdot g^{-1}$, and low D/G bands ratio in the Raman spectra. Mesopore presence accounts for the fast formation of the double layer and the decrease of resistive properties which implies increased power properties referred to activated carbons. Symmetric carbon/carbon devices can provide energy densities 7-9 $Wh \cdot kg^{-1}$ and maximal powers higher than 50 $kW \cdot kg^{-1}$. These values compare well with 9 $Wh \cdot kg^{-1}$ and 26 $Wh \cdot kg^{-1}$ furnished by activated carbons. Nevertheless, such TMCs show two major issues for performing better than activated carbons in aqueous electrolyte capacitors. Firstly, they show surface carbon functionalities, narrowing the electrochemical window of the capacitor and decreasing the capacitor cycling life. Secondly, pore saturation is evidenced in these systems, unlike activated carbon, showing higher specific surface area and micropores content. Under prolonged cycling, our TMC electrode performance is poorer than that of activated carbon. However, mesoporosity positively affects the electrode response against increasing power. Beyond a power of 1.4 $kW \cdot kg^{-1}$, only TMCs provide stable energy densities (> 6.5 $Wh \cdot kg^{-1}$), comparable or higher than those observed for activated carbons in corrosive electrolytes.

Keywords: templated mesoporous carbons, electrochemical capacitors, electrodes, electrochemical impedance spectroscopy

1. Introduction

Since the discovery of environmental issues associated to the use of fosil-fuel based energy, special attention has been paid to the development of electrochemical energy storage devices. In this context, lithium ion batteries and supercapacitors have been proposed for satisfying future energy demands [1,2]. Conventional capacitors can sometimes ~~show~~ deliver a specific power higher than 1000 $kW \cdot dm^{-3}$ but very low energy density. Higher energies can be obtained ~~reached~~ by increasing the capacitance or the operating voltage of the devices. When the values of capacitance surpass 100 $F \cdot g^{-1}$, whatever the mechanism of charge storage, the devices (called supercapacitors, ultracapacitors or electrochemical capacitors) fill the gap between those providing high energy but low power (batteries) and those furnishing high power but low energy (traditional capacitors) [3]. Furthermore, because of the particular charge storage mechanism, capacitors are known to show a long cycling life (one million cycles or more) [2,3]. Other technological advantages are: fast charge/discharge time (a few miliseconds to a few seconds), high coulombic efficiency and environmental goodness if no corrosive electrolytes (H_2SO_4, KOH) are present in the device.

In an electrochemical capacitor, charge is stored in the electrode/electrolyte interface. Depending on the mechanism of charge storage, two different kinds of capacitors have been proposed [2,4]. When charge is stored through the thin double layer formed by the electrolyte ions distributed in parallel to a polarized electrode surface, they are called electrochemical double layer capacitors (EDLC). The charge is in this case strongly dependent on the surface available to the electrolyte ions and on the electrolyte concentration. Typical EDLC electrodes are carbonaceous materials: activated carbons, carbide-derived carbons, carbon fiber and aerogels…The second mechanism for charge storage implies the use of transition metal oxides and polymers as electrode materials. Unlike for EDLC, charge is stocked by means of fast redox reactions (usually called pseudo-faradaic reactions) taking place at or near the

electrode material surface. For this reason they are called electrochemical pseudocapacitors. A real charge transfer process occurs at the electrode/electrolyte interface and a redox reaction modifies the structure and properties of the electrode material, at least at surface level. Therefore, cycling life of pseudocapacitors is generally shorter than for EDLC. Regarding the electrolytes, they are based on aqueous or organic solutions, with different electrochemical voltage windows and as a consequence, distinct values of energy and power.

Equation **(1)** correlates the typical double layer parameters (thickness (t), surface (A) and dielectric constant (ε)) to the capacitance, C, provided for an electrode.

$$C = (\varepsilon\varepsilon_0 A)/t \qquad \textbf{(1)}$$

~~Apparently~~, According to **(1),** the higher the electrode surface the bigger the capacitance value~~s~~. However, recent studies on activated carbons have shown that there is no linear relationship between the surface specific area and the capacitance [5-12]. A pore size distribution in the range of 2-5 nm, which is larger than the size of two solvated ions, was identified as a way to improve the energy density and power capability [9,13-15]. Later, Chmiola et al. [16] showed that ions can desolvate and accommodate in the subnanometer ($0.5\ nm < d_{pore} < 1\ nm$) porosity leading to dramatic increase of the capacitance. Equation **(2)** has been proposed to determine the value of the capacitance in the mesopores ($d_{pore} > 2\ nm$):

$$C = (\varepsilon\varepsilon_0 A) /[b \cdot \ln(b/(b-d))] \qquad \textbf{(2)}$$

where b and d are the pore radius and the distance of approach of the ion to the carbon surface respectively.

The use of mesoporous materials [5,17] accounts for a net improvement of the properties of the surface exposed to the electrolyte, in terms of increased surface area, mono-modal distribution of pores, among other textural characteristics, as well as for the fact that the

materials are generally constituted of nanoparticles, decreasing the lithium ion path and increasing particles connectivity. The wide literature on the application of mesoporous materials for electrochemical capacitors deals with the use of EDLC, mainly based on carbonaceous materials [5-9,18]. As a matter of fact, the claimed capacitance originating from nanopores [16,19-23] has decreased the interest in investigating mesoporous materials. However, Frackowiack et al. [6] pointed out that even if the micropores play an essential role for ions adsorption, the mesopores are necessary for their quick transportation to the bulk of the materials. They stated that under polarization, the solvated ions migrate easily in the mesopores (playing the role of corridors) until reaching the entrance of micropores, being then desolvated to adapt to the pore size. In a typical activated carbon, the situation differs. The pathway of solvated ions to reach the active surface is very tortuous and long, with several bottle-necks. According to this, mesoporous carbons have been prepared with the hard template technique (by using MCM-48, SBA-15, MSU-1 among others), introducing preferentially sucrose into the voids as carbon precursor [6,12,18,24-28]. The resulting Templated Mesoporous Carbons (TMC) have single modal distribution of pores, centered in 2.5-4 nm range. One of these TMC (CMK-3) excels in capacitive properties (170 $F \cdot g^{-1}$ [6] or 200 $F \cdot g^{-1}$ [18] in organic or aqueous (acid or basic) electrolyte respectively). It should be mentioned that current research on TMC is focused on: i) surface-modified carbons with nitrogen- or oxygen- functional groups, in order to introduce pseudocapacitance and improve the surface wettability [29,30], ii) testing in corrosive electrolytes [28-35] and/or iii) activation with KOH, H_2SO_4 or other agents in order to enhance the microporosity of the carbon [31,33-35].

In this work we present new TMC, derived from two mesoporous templates: Plugged Hexagonal Templated Silica (PHTS) and Mesostructured Cellular Foam (MCF). Their textural, morphological and electrochemical properties are therein discussed and compared

with those of activated carbon NORIT, a capacitor electrode material. Our results indicate that TMC could provide higher maximal powers (64 and 53 $kW \cdot Kg^{-1}$ for C-MCF and for C-PHTS, respectively, versus 26 $kW \cdot Kg^{-1}$ for NORIT). However, higher values of specific surface area and micropores volume, as well as lack of pseudocapacitive phenomena, result in a better maintenance of energy of the device built with NORIT after 500 cycles: 8.9 $Wh \cdot Kg^{-1}$ versus 7.7 and 6.5 $Wh \cdot Kg^{-1}$ for C-MCF and for C-PHTS, respectively. Nevertheless, capacitive response is extremely dependent on the power to which the device is submitted. Thus, energy densities are almost constant for C-MCF (7.7 $Wh \cdot Kg^{-1}$) and C-PHTS (6.6 $Wh \cdot Kg^{-1}$) electrodes at a power of 2.6 $W \cdot Kg^{-1}$, whereas NORIT electrode provides 5.5 $Wh \cdot Kg^{-1}$ at similar power. At such high powers, only activated carbons or activated TMCs, tested in corrosive electrolytes, perform better than our electrode materials.

2. Experimental

Plugged Hexagonal Templated Silica (PHTS) consists of hexagonally ordered mesopores with diameters similar to those of SBA-15 [36]. Pore walls are 3-6 nm thick and perforated with micropores, therefore PHTS is a material combining micro- and mesopores. PHTS also possesses microporous amorphous nanoparticles (plugs) in the uniform mesoporous channels resulting in higher micropore volumes. The pillaring effect of the nanoparticles gives PHTS a higher mechanical stability compared to pure SBA-15.

For the synthesis of PHTS, 15 g of TEOS are added to a solution containing 4 g of P123 ($EO_{20}PO_{70}EO_{20}$ copolymer), 130 ml of distilled water and 20 ml of concentrated HCl (1TEOS: 2.77HCl:192 H_2O:0.008 P123 molar ratios). After heating at 60ºC under stirring for 7.5 h, the mixture is transferred to an oven at 80 ºC and old for 15.5 h. Finally a white solid is recovered, filtered, washed with distilled water and dried at r.t. In order to remove the template, the product is heated under air at 550 ºC for 6 h with a gradient of $1^{o}\ C \cdot min^{-1}$.

Mesostructured Cellular Foam (MCF) is obtained by addition of a swelling agent (in this case, mesitylene (1,3,5-trimethylbencene) to the synthesis of SBA-15 [36]. The swelling agent produces a sponge-like foam with 3D structure consisting of uniform spherical cells 15-50 nm large, accessible via large windows (5-20 nm). MCF is a very open structure with large uniform pore diameters, thick pore walls and large pore volumes. For the synthesis of MCF, 4 g of P123 and 20 mL of concentrated HCl are dissolved in 130 ml of distilled water. 0.0467 g of NH_4F and 4.6 mL of mesitylene are added to the solution and the whole mixture stirred at 35-40 ºC. After one hour, 9.14 ml of TEOS (1 TEOS: 5.87 HCl: 194 H_2O: 0.017 P123: 0.031 NH_4F: 0.815 mesitylene molar ratios) are added and the mixture is stirred for 20 h. After transferring to an oven at 100 ºC under vacuum for 24 h, the mixture is allowed to cool. The product is filtered and washed three times with distilled water. Template is finally removed through the same treatment used for PHTS.

For the preparation of TMC, 1.25 g of sucrose and 0.145 g of sulfuric acid are dissolved in 5 ml of distilled water. 1 g of the mesoporous silica is added to this solution for one hour, with the assistance of ultrasounds. The mixture is dried in an oven at 100 °C for 12 h and then at 160 °C for 24 h. The formed carbon/silica composite is graphitized by a thermal treatment at 900 °C under a nitrogen atmosphere for 20 h. After cooling, the silica is removed by treating the resulting powder with HF, centrifuging and thoroughly washing it with distilled water.

X-rays diffraction (XRD) patterns were obtained with a Phillips X'PERT MPD diffractometer equipped with a Cu-Kα source. Small angle measurements were performed in a 2θ range from 1 to 5º. Transmission electron microscopy (TEM) images were obtained on a PHILIPS TECNAI-10 electronic microscope operating at 200 kV. Scanning electron microscopy (SEM) images were obtained with a Jeol 6300 microscope. Textural properties were established from nitrogen adsorption/desorption isotherms on a MicromeriticASAP 2020 instrument using nitrogen gas as adsorbate. Pore size distribution was calculated by applying

the Barret et al. method to the desorption branch of the isotherms. Raman measurements were carried out with a Renishowin Vida Microscope, a Renishaw CCD Camera (578x400) detector and with a 785 nm edge laser in Linefocus mode, working in a 100 to 1700 cm^{-1} wavenumber range. The power of the laser beam used on the sample was 0.1 or 5 mW.

Electrode mixture was prepared by mixing the carbon, teflon (water suspension 60% weight, *Aldrich*) as a binder and carbon black (Super P, *Timcal*) as a conductive additive. Firstly the polymer is dissolved in hot ethanol and then carbons are added to the solution, keeping a w/w/w ratio of 80:10:10. After slowly heating the mixture, a slurry is obtained. The slurry is subsequently casted on a glass surface, modelled as a film, recovered and dried at 80 °C for 2 h. Voltammetric and electrochemical impedance spectroscopy (EIS) measurements were controlled via a Autolab (Ecochemie model Pgstat20) instrument connected to a PC computer with suitable software (GPES). A three electrodes cell was used for these tests. Squared (1 cm^2) slices of the carbon film were used as working electrodes. Counter electrode consisted of a platinum gauze (*Aldrich*, 99.99%). Reference electrode was Ag/AgCl ($E^0_{(25°C)}$= +0.199 V vs NHE). The spectra were obtained over the 84 kHz–3.4 mHz frequency range. The AC signal was 10 mV peak to peak. Impedance diagrams were fitted by employing the Zplot® software, from Scribner Associates. Galvanostatic tests were carried out in an Arbin multichannel in symmetric cells containing NORIT or TMC as both electrodes. Specifications of the CV and galvanostatic measurements are given in the *Electrochemical tests* section of this paper.

The values of capacitance are determined by using the formula

$$C = I/(dV/dt) \qquad \textbf{(3)}$$

where I is the observed intensity (mA) developed between the working and the counter electrode, and dV/dt ($mV \cdot s^{-1}$) corresponds to the constant voltage steps applied. This formula

yields the capacitance of one electrode in a three-electrode configuration and that of a symmetric device. Specific capacitance (C_{sp}) associated to the device was calculated according to:

$$C_{sp} = 2\ C/\ m \qquad \textbf{(4)}$$

where C is the device capacitance and m is the weight of one electrode.

In order to obtain realistic energetic parameters we employed the formulae associated with the real values of energy and power delivered by the devices under galvanostatic regime [37]. These formulae provide data to a realistic discussion of TMC as suitable electrodes in ECs.

Real power, P_{real}, is defined by:

$$P_{real} = \Delta E\ I/\ m\ (W \cdot Kg^{-1}) \quad \textbf{(5)}$$

where $\Delta E = ½\ (E_{max}+E_{min})$ and E_{max} and E_{min} are the potentials after the end of charge and discharge, respectively. Real energy, E_{real}, can subsequently be calculated by multiplying power by the discharge time, t (seconds) according to:

$$E_{real} = P_{real}\ t/\ 3600\ (Wh \cdot Kg^{-1}) \quad \textbf{(6)}$$

For fruitful discussion, maximal power, P_{max}, is also calculated employing the equation:

$$P_{max} = V^2/4\ ESR\ (W \cdot Kg^{-1}) \quad \textbf{(7)}$$

where $V=E_{max}$-IR (ohmic drop) and ESR is the electrical series resistance deduced from EIS measurements.

3. Results and discussion.

3.1. Physicochemical characterization

Figure 1 contains the XRD patterns corresponding to the different mesoporous material synthesized in this work: PHTS, C-PHTS, MCF and C-MCF. PHTS pattern is consistent with a well ordered pores structures, providing three peaks at 0.94°, 1.62° and 1.88° 2Θ corresponding to the [100], [110] and [200] planes, respectively. According to the C-PHTS diffractogram, pores order is severely altered during the preparation of the carbon derivative, and consequently, only a peak at 1.09° 2Θ with less intensity (1/20) is observed. In the case of MCF and C-MCF, weak and ill-defined features are distinguished. As a consequence of the large size of the pores, a first order peak should be found below 0.2° 2Θ.

TEM images corresponding to the different mesoporous systems are collected in Figure 2. A remarkable ~~a~~ morphological resemblance exists between each pristine silica and its replica. Thus, PHTS consists of smooth rods [36,38] containing curved mesopores following an ordering pattern, consistent with the XRD results of Figure 1. However, the treatment leading to C-PHTS enhances the curvature of the pores and deteriorates their order. Regarding MCF and C-MCF, both materials are sponge-like shaped [36] and contain pores larger in size and more randomly disposed than in PHTS/C-PHTS. A clear ordering pattern is not evidenced, which is consistent with the weak and broad diffractogramm presented in Figure 1**.**

Nitrogen adsorption/desorption isotherms for TMC (Figure 3) confirm the mesoporous character of these solids, (type IV in the IUPAC definition). However, the chemical and thermal process involved in their fabrication has largely contributed to significant variations from the pristine silica profiles [36]. For instance, the vanishing of the plugs in C-PHTS cancels the second desorption step. Besides, in the preparation of C-MCF, pores of large size are formed and isotherms contain a new step in both branches. For comparison purposes, Figure 3 also shows the isotherm for NORIT, a microporous carbon which is a standard EDLC material. Its isotherm belongs to the IUPAC type I, corresponding to the

adsorption/desorption of one monolayer of nitrogen in the system nanopores. As a consequence, no hysteresis is observed for this material.

C-PHTS shows a very narrow pore distribution centered in 2.5 nm (Figure 4), a value close to the average pore size collected in Table 1. Although C-MCF mainly developed two very narrow pore sizes in the 2.25-3.05 nm range, pores as large as 14.6 nm are also formed. Therefore, C-MCF shows the larger average pore size [36]. Similar to C-PHTS, NORIT carbon shows a narrow distribution centered in 2.4 nm. Other noteworthy properties such as the specific surface area and the pores volume are collected in Table 1. There is a relevant increase of the first parameter from the pristine silica to the TMC (850 and 640 m^2/g for PHTS and MCF respectively) but specific surface area values remain smaller than that of NORIT. The observed pore volumes, with a weak contribution of micropores, also confirm the mesoporous character of C-PHTS and C-MCF.

Raman spectroscopy is a powerful tool for the characterization of carbonaceous materials. Selected Raman spectra for the TMC and NORIT are collected in Figure 5. The spectra corresponding to the TMC can be fitted to four components, the maximum of which appear at 1194, 1340, 1510 and 1580 cm^{-1}, respectively [10]. NORIT spectra contain an additional weak component at 1442 cm^{-1}. The two bands at 1580 cm^{-1} and 1340 cm^{-1} are assigned to the E_{2g} and A_{1g} graphite modes, called G and D band, respectively [39]. The D band is related to the breakage of symmetry occurring at the edges of graphite sheets. Therefore, the relative intensity of D and G bands is associated with the structural disorder. Furthermore, the bands at 1194 and 1510 cm^{-1} are assigned to tetrahedral and sp^3-type carbon with smaller conductivity observed in highly amorphous carbonaceous materials [39]. The band at 1420 cm^{-1} has also been identified in multiwalled carbon nanotubes without a suitable attribution [40]. A smaller D/G ratio correlates to a higher conductivity. The values of D/G ratio for the

various carbons are collected in Table 1 and reveal good conductivity properties for the C-PHTS material.

Information about the groups in TMC surfaces can be obtained by X-rays photoelectron spectroscopy (XPS). C 1s XPS spectra (Figure 6) contain a main peak at 284.6 eV, related to C=C bonds in the carbon. Despite the fact that our TMC have not been activated after synthesis, oxidized carbon species (-C-OR at 285.6 eV [32,41]) are noticed in the XPS profiles. C-MCF also shows -O-C=O functionalities leading to a peak at 287.2 eV [32,41]. A contribution to the C 1s profile at 289.3 eV is also evidenced and can be ascribed to C=C bonds observed in highly crystallized graphite [41] or to O-C=O functionalities [32]. The later assignation seems more suitable as the temperature of synthesis is relatively low for promoting the formation of well-ordered graphite. According to this, the relative amounts of surface functionalities are: 44.5% and 28.3% C-O-R for C-MCF and C-PHTS, respectively; 15.3% and 22.2% O-C=O for C-MCF and C-PHTS, respectively and finally, 3.5% of C=O for C-MCF. To sum up, C-MCF material contains larger contributions (63.3% versus 50.5% for C-PHTS) of those oxidized carbon species, which can be electroactive and responsible of a pseudocapacitance.

Electrochemical tests

Electrochemical tests have been carried out on aqueous K_2SO_4 solutions. Choice of a neutral sulfate is based on the suitable properties of such salts [42] to replace corrosive electrolytes (KOH, H_2SO_4) of common use in EDLC [28-35]. Figure 7 shows the adaptation of a typical first voltammetric cycle (CV, I/V profile) in 0.5M K_2SO_4 solution to a capacitance/V profile by using the formula (**3)**. The NORIT-based cell shows a slight deviation from the typical box shape of an EDLC. This deviation, evident when the electrode polarizes negatively, reflects

the different characteristics for the anion (positive polarization) and cation (negative polarization) adsorption and diffusion, these processes being hindered for the cation [2,4]. The average pore size for NORIT, close to 2.2 nm is in fact below the hydrated potassium ion radius (3.31 nm) although potassium ion can partially desolvate to enter in the micropores (unhydrated radius 1.49 nm). Conversely, upon positive polarization and anions adsorption, the profile is more similar to a box. Furthermore, for NORIT electrode, electrochemical window is -0.9 and +0.8 V vs Ag/AgCl.

CV profiles of TMC electrodes contain broad bands at -0.2 V which seem to indicate the presence of functional groups as above mentioned in section 3.1. Therefore, its I/V profile is a mirror of the presence of carbon functionalities [29,43]. After the development of those broad anodic bands, CV profiles at low voltages indicate once again the difficulty in the cations adsorption, which agrees with a pore size close to 2.5 nm detected for both TMCs, not too far in value from that observed for NORIT. Expected influence of larger size pores observed in the BET curves is missed. During the positive polarization, both TMC profiles contain a broad oxidation band associated to the reversibility of the above mentioned reduction process with an additional band located at +0.3 V for C-PHTS. Due to the carbon functionalities, TMCs prepared in this work are less stable upon positive polarization. A suitable cathodic limit for our tests was set to +0.55 V.

It has been stated that the electrochemical stability of carbon functionalities can be limited and thus, the electrochemical cycling can result in a loss of capacity [2,4]. Furthermore the average capacitance of the carbons is 80, 75 and 65 $F \cdot g^{-1}$ for NORIT, C-MCF and C-PHTS respectively. These values are lower than expected for activated carbons, reflecting a change in the materials porosity during the assessment of the electrodes [30]. However, the performances are consistent with a lesser value of surface area and smaller content in micropores of the TMCs compared to NORIT.

Despite these poorer capacitance values, we examined the accessibility of the porous active layer for the TMC and NORIT surfaces, by carrying out EIS experiments. Figure 8 shows a Bode diagram (therein as log $(1/Z_{im}\cdot\omega)$ vs log (ω) , where Z_{im} and ω correspond to imaginary part of the system impedance and the angular frequency, respectively). The low frequencies values of the log $(1/Z_{im}\cdot\omega)$ ratio correspond to the highest capacitance that a system can develop and to the double layer capacitance times the total pore surface area [2,4]. The higher the frequency for which the capacitance is maximal, the thinner the active layer for the development of the electrochemical double layer. As the path crossed by the electrolyte ions to reach the micropores is tortuous [4,28], the activated carbon NORIT provides the smallest capacitance at higher frequencies (Figure 8). On the contrary, C-MCF and C-PHTS establishes more rapidly the electrochemical double layer, consistent with the presence of mesopores where electrolyte ions diffusion is facilitated. However, if the electrolyte ions are allowed to penetrate deeply (in the Bode plot, at the lowest frequencies), the active layer offered by the NORIT activated carbon provides a superior capacitance. As EIS experiments approach the equilibrium, the capacitance values calculated by EIS are always larger than that obtained by CV (approximately 5-7 $F\cdot g^{-1}$). Despite their different textural and conductivity properties, NORIT and C-PHTS develop a similar value of "equilibrium" capacitance, consistent with some similar pore properties. Referred to the total pore surface area, the reported double layer capacitance are similar for both mesoporous carbons, 6.2 $\mu F\cdot cm^{-2}$, whereas NORIT provides 5.7 $\mu F\cdot cm^{-2}$ [18].

Prompted by these interesting results, we built symmetric devices containing positive and negative electrodes with identical amounts of the same carbon. The voltage limits were fixed by those presented by the TMCs, i.e. -0.9 V (when acting as negative electrode) and +0.55 V (when acting as positive electrodes). Cycling in the 0-1.45V was initially done under galvanostatic regime of 0.5 $A\cdot g^{-1}$.

Figure 9 shows the 1st (after five activation voltammetric cycles) and 500th galvanostatic cycles for the NORIT and TMCs. For an ideal capacitor, with constant capacitance value, the profile of a V/t curve should be a straight line with slope equal to I/C (I= applied intensity, C= device capacitance) during charge and discharge. Therefore, the NORIT carbon electrochemical behavior is almost ideal. Up to 1.3 V, both TMC also behave ideally but for higher voltages a curvature is noticed, consistent with bands appearing at their CV profiles at voltages close to +0.55 V and -0.9 V (Figure 7), associated to the presence of functional groups [28,29,42]. NORIT electrode develops an ohmic drop of 100 mV followed by a close to ideal linear V/t variation. TMC electrodes show a smaller ohmic drop (70 mV), revealing advantageous power properties. Upon discharge, a deviation from linear variation reveals pores saturation in TMC electrodes [4]. Another feature in Figure 9 is the charge/discharge time. The longer time for NORIT indicates a higher value of capacitance than for TMCs.

After 500 cycles NORIT-based devices show the same features (I/t profile and charge/discharge time). On the contrary, both TMC electrodes decreased the crossing charge time, indicating a loss of capacitance upon cycling. Furthermore, C-MCF still deviates from the ideal behavior beyond 1.3 V indicating the maintenance of the pseudofaradaic process. Conversely, these phenomena are cancelled in C-PHTS and its charge profile is close to the ideal behavior after cycling. Furthermore, discharge profiles are in line with a pronounced saturation of the pores in the case of C-MCF.

The three systems were voltammetrically cycled after stopping at selected galvanostatic cycles (Figure 10). The CV curves indicate that the NORIT electrode requires an initial activation. Indeed, NORIT carbon features a thick active layer constituted of micropores, which requires more time to be accessed by the electrolyte ions. After such activation, the CV profile of NORIT is close to the box shape during 2000 cycles, keeping a constant area (and therefore, a constant capacitance) under the anodic or the cathodic waves. As expected, TMCs

showed a different behavior to NORIT, not requiring activation for yielding their maximal capacitances. Moreover, voltammetric curves decrease upon cycling, indicating a continuous capacitance loss. Interestingly, C-PHTS profile is close to the ideal box behavior upon cycling with only a deviation at 2000 cycles close to the voltage limits. This feature was justified by Conway et al. [2] as electrolyte starvation or by Béguin et al. [4] among other authors, as pores saturation. Deviation from ideal box profile is especially remarkable for the C-MCF based electrode (Figure 10) due to the above mentioned pore saturation and surface carbon functionalities.

The evolution of the capacitance versus the number of cycles is shown in Figure 11. Seemingly, carbon conductivities are not affecting the electrochemical behavior of our electrodes. The rank $C_{NORIT} > C_{C\text{-}MCF} > C_{C\text{-}PHTS}$ is maintained up to 2000 cycles and follows the surface area and the micropore volume trend. A minor amount of micropores volume combined with a smaller surface area account for the pore saturation leading to capacitance fade. Additionally, presence of functional surface groups explains the deterioration of electrochemical properties of the C-MCF electrode. Besides, the pseudocapacitance contribution seems to be cancelled for the C-PHTS electrode after several cycles.

Table 2 collects the capacitance and real energy values for the three devices at the first cycle and after 500 cycles. Additionally, equivalent series resistance (ESR) and maximal power values are also collected. Values obtained for NORIT are similar to that expected for other activated carbon, and reveal low energy and high power densities of an electrochemical capacitor. For this particular activated carbon, energy density is close to 10 $Wh \cdot kg^{-1}$, which is similar to that shown by C-MCF and higher than that of C-PHTS, due to the smaller capacitance of the latter.

The observed capacitance trend is initially against the use of our TMC as electrodes. Nevertheless, as smaller charge transfer resistance, and faster electrolyte ions diffusion is expected for the mesoporous systems, the power provided by mesoporous materials-based devices should be higher. Thus, a pertinent result in order to reveal the interest of mesoporous materials for electrochemical capacitor applications is the power density. By virtue of a lower ESR, TMC electrodes develop a high maximal power density (> 50 $kW \cdot kg^{-1}$), at least twice the density furnished by activated carbon (26 $kW \cdot kg^{-1}$). However, as capacitance fades upon cycling for TMCs, energetic parameters fade for such devices. For instance, energies are in average 11% lower at the 500^{th} cycle whereas NORIT energy is stable.

Ragone plot for the different carbon electrodes is shown in Figure 12. At relatively low currents (0.05 $A \cdot g^{-1}$ corresponding to a power close to 33 $W \cdot kg^{-1}$), energy densities provided by C-MCF electrode are similar to that of activated carbon (10 $Wh \cdot kg^{-1}$). On the contrary, C-PHTS capacitance is only a 77% of such value. Increasing the current regime leads to disparate electrodes behavior. Thus, energy density is maintained for the NORIT electrode and decreases for the TMCs, until a power higher than 1.4 $kW \cdot kg^{-1}$ is tested. These sequences reveal a reduction of the TMCs capacitance upon cycling at such regimes, due to the lower specific surface area and micropores volume, compared with NORIT. After submitting the devices to 1.4 $kW \cdot kg^{-1}$, C-MCF and C-PHTS electrodes stabilize to almost 8 $Wh \cdot kg^{-1}$ and 7 $Wh \cdot kg^{-1}$, respectively, whereas NORIT starts to fade, which indicates the interest on developing TMC supercapacitor electrodes. Retention of energy density of the C-PHTS electrode agrees with the role of well-ordered mesopores structures under increasing powers [43]. For comparison, Table II collects some recent supercapacitors electrodes performances. Note that the highest values of energy densities correspond to systems tested in a three electrode configurations [32,35] and not in a symmetric capacitor. Due to the use of a high surface area counter electrode (Pt) in the three electrode configuration, charge stored is higher

and ESR is smaller in the device, both factors resulting in higher energy densities. Our TMC electrodes provide higher or similar energy densities than those furnished by Ordered Mesoporous Carbons (OMC) in KOH electrolyte [28,32] and activated carbon in KOH or H_2SO_4 electrolyte [28,34].

As pore saturation and carbon functionalities can account for the poorer electrochemical properties of our TMCs upon long cycling and modest powers, we prompted to continue our study building devices with organic electrolytes, based on a solution of NEt_4BF_4 in acetonitrile. In such electrolyte, the lack of protons precludes the pseudocapacitive behavior of the TMCs. Furthermore, NEt_4^+ cation and BF_4^- anion radii are two or three times smaller than that of K^+ and SO_4^{2-} and therefore, pores saturation should be more limited than in the aqueous electrolyte. Additionally, the use of organic electrolytes boosts the device energies by expanding the voltage limits to at least 2V.

The advantage of working with organic electrolyte is confirmed by the form of cyclic voltammetries in 1.5M NEt_4BF_4 (CH_3CN) shown in Figure 13. Symmetric devices based in the three carbons presented similar cyclic voltammetries following a profile very close to the ideal box. Interestingly, pore saturation is only distinguishable for carbon activated at limit voltages. Furthermore, C-MCF and C-PHTS curves do not (or slightly) contain bands associated to surface carbon functionalities. Finally, C-MCF yields same capacitances than NORIT. The smaller microporous volume and specific surface area still account for lower capacitance values of C-PHTS. These preliminary results let us believe that the TMCs studied here would be advantageous in relatively high voltage capacitors with organic electrolytes. Further efforts are now being carried out in order to evaluate and to optimize their electrochemical performances by increasing surface area and through introduction of microporosity by alkali activation.

4. Conclusion

Two templated mesoporous carbons (C-MCF and C-PHTS), obtained from mesoporous silica and without an activation step, are for the first time reported as electrodes for electrochemical capacitors in aqueous neutral electrolytes. Their properties are compared with activated carbon NORIT.

XRD and TEM observations indicate that carbon replicates are morphologically similar to the pristine template silica with C-PHTS, exhibiting an ordered pore structure. TMCs showed specific surface area higher than 1000 $m^2 \cdot g^{-1}$ and mainly mesoporosity with a narrow pore size distribution for C-PHTS, centered close to 2.5 nm and larger distribution for C-MCF. Raman spectroscopy suggests suitable conductivity properties for both TMCs, especially for NORIT. Carbon functionalities are detected in the TMCs by XPS, which predicts a pseudocapacitance for such electrodes. In fact, voltammetric profiles contain broad bands in the (-0.6 V, +0.2 V) range. Presence of these surface active groups account for narrower electrochemical window compared to NORIT.

Capacitance values observed for the three carbon electrodes indicate the strong influence of specific surface area and micropores volume. Therefore, activated carbon NORIT, showing bigger values of these textural parameters yields higher capacitance (80 $F \cdot g^{-1}$ vs 75 and 65 $F \cdot g^{-1}$ for C-MCF and C-PHTS, respectively). Nevertheless, EIS reveals that due to advantageous textural properties, TMCs create the double layer faster than activated carbon does. In turn, when a symmetric carbon/carbon device is built, NORIT provides higher retention of capacitance upon cycling, due to the limited pore saturation (in agreement with the above mentioned textural properties) and the lack of pseudocapacitance.

As ohmic drop and ESR are smaller than for NORIT, maximal power is higher for TMCs. However, Ragone plots indicate that at modest powers, the capacitors built with TMC provide

similar or smaller energy densities than with activated carbon. The positive effect of mesopores presence is only evidenced at high powers. For example, C-MCF and C-PHTS electrode provides a stable energy density of 7.8 $Wh \cdot kg^{-1}$ and 6.6 $Wh \cdot kg^{-1}$, respectively, beyond P=1.4 $kW \cdot kg^{-1}$. NORIT electrode (among other activated carbons [28]) capacitance declines at that power. Therefore, the performances of our not activated TMCs in non-corrosive electrolytes are suitable for safe and high power supercapacitor purposes.

We also observe that our TMCs behave in a similar way to NORIT in an organic electrolyte. These features can be explained by cancellation of the pseudocapacitance, as protons are not available in the electrolyte and by a better match between pores size and electrolyte ions radii, decreasing pore saturation. Taking into account that our TMCs are not activated, these last results reveal that they can be useful for high power devices with organic electrolytes.

5. Acknowledgements

This work was supported by MICINN (MAT 2010-16440). Authors are indebted to Dr. Manuel Mora (Department of Organic Chemistry, University of Córdoba) for recording the Raman spectra, Pr. M.T. Pineda and M. Blázquez (Department of Physical Chemistry, University of Córdoba) for allowing the use of Autolab equipment. Finally, F. Gracia (Transmission Electronic Microscopy and Scanning Electronic Microscopy Services, S.C.A.I.) and J.I. Corredor (Analysis Service, SCAI) of the University of Córdoba for TEM examinations and XPS measurements respectively.

Legend of Figures.

Figure 1. XRD patterns of the mesoporous materials prepared in this work: PHTS, C-PHTS, MCF and C-MCF.

Figure 2. TEM images of the mesoporous materials prepared in this work.

Figure 3. Nitrogen adsorption/desorption isotherms for the template mesoporous carbons prepared in this work and NORIT carbon.

Figure 4. Pores distribution in the TMC and NORIT materials, calculated from the desorption branch by using the BJH method.

Figure 5. RAMAN spectra (fitting included to four or five components) of the carbons studied in this work.

Figure 6. XPS spectra (fitting included to three or four components) of the TMCs studied in this work.

Figure 7. First voltammetric cycle of the carbons studied in this work in 0.5M $K_2SO_{4(aq}$. Voltage steps = 20 $mV \cdot s^{-1}$. Counter electrode: Pt. Reference electrode: Ag/AgCl.

Figure 8. Bode diagramm for the TMCs and NORIT studied in this work.

Figure 9. First and 500^{th} galvanostatic cycle (I=0.5 $A \cdot g^{-1}$) of the symmetric capacitor based on NORIT and TMC-based electrodes .

Figure 10. Cyclic voltammogramms corresponding to symmetric capacitors based on carbon electrodes after 5, 500 and 2000 cycles under 0.5 $A \cdot g^{-1}$.

Figure 11. Capacitance versus number of galvanostatic cycle (I=0.5 $A \cdot g^{-1}$) of the symmetric capacitors with NORIT and TMC-based electrodes.

Figure 12. Ragone plots for the symmetric capacitors with NORIT and TMC-based electrodes.

Figure 13. Fifth voltammetric cycle of the symmetric capacitors based on carbons (NORIT, C-MCF,C-PHTS) in 1.5M NEt_4BF_4 (CH_3CN). Voltage steps = 20 $mV \cdot s^{-1}$.

References

[1] B. Scrosati, J. Garche. *J. Power Sourc.* 195 (2010) 2419-2430.

[2] B.E. Conway, *Electrochemical supercapacitors*, Plenum Publishing, New York, 1999.; R. Kötz, M. Carlen, *Electrochim. Acta* 45 (2000) 2483-2498.

[3] *Interface*, 17(1) (2008) 33-53.

[4] F. Beguin and E. Frackowiak Eds. Supercapacitors. Materials, Systems and Applications, Wiley V-CH (Weinheim, Germany), 2013 (ISBN 978-3-527-32883-3).

[5] P. Simon, Y. Gogotsi, *Nature Mat.* 7 (2008) 845-854.

[6] C. Vix-Gurtel, E. Frackowiak, K. Jurewicz, M. Friebe, J. Parmentier, F. Béguin, *Carbon* 43 (2005) 1293-1302.

[7] H. Shi, *Electrochim. Acta* 41(1996) 1633.

[8] D. Qu, H. Shi, *J. Power Sourc.* 74 (1998) 99.

[9] O. Barbieri, M. Hahn, A. Herzog, R. Kotz, *Carbon* 43(2005) 1303-1310.

[10] M. Endo, T. Maeda, T. Takeda, Y.J. Kim, K. Koshiba, H. Hara, M.S. Dresselhaus, *J. Electrochem. Soc.* 148 (2001) A910.

[11] S. Shiraishi, H. Kurihara, L. Shi, T. Nakayama, A. Oya, *J. Electrochem. Soc.* 149 (2002) A855.

[12] T.A. Centeno, M. Sevilla, A.B. Fuertes, F. Stoekli, *Carbon* 43 (2005) 3012-3015.

[13] C.H. Kim, S.I. Pyun, H.C. Shin, *J. Electrochem. Soc.* 149 (2002) A93.

[14] E. Frackowiak, F. Beguin, *Carbon* 39 (2001) 937.

[15] G. Salitra, A. Soffer, L. Eliad, Y. Cohen, D. Aurbach, *J. Electrochem. Soc.* 147 (2000) 2486.

[16] J. Chmiola, G. Yushin, Y. Gogotsi, C. Portet, P. Simon, P.L. Taberna, *Science* 313 (2006) 1760-1763.

[17] F. Cheng, Z. Tao, J. Liang, J. Chen. *Chem. Mater.* 20 (2008) 667-681.

[18] F. Lufrano, P. Staiti, *Int. J. Electrochem. Sci.* 5 (2010) 903-916.

[19] R. Dash, J. Chmiola, G. Yushin, Y. Gogotsi, G. Laudisio, J. Singer, J. Fischer, S. Kuycheyev, *Carbon* 44 (2006) 2489.

[20] G. Laudisio, R. Dash, J.P. Singer, G. Yushin, Y. Gogotsi, J.E. Fischer, *Langmuir* 2006, 8945.

[21] R. Mysyk, E. Raymundo-Piñeiro, F. Beguin, *Electrochem. Comm*. 11 (2009) 554.

[22] R. Mysyk, E. Raymundo-Piñeiro, J. Pernak, F. Beguin, *J. Phys. Chem. C* 113 (2009) 13443.

[23] R. Mysyk, Q. Gao, E. Raymundo-Piñeiro, F. Beguin, *Carbon* 50 (2012) 3367.

[24] H. Tamai, M. Kouzu, M. Morita, H. Yasuda, *Electrochem. Solid State Lett*. 6 (2003) A214.

[25] Y. Yamada, O. Tanaike, T.T. Liang, H. Hatori, S. Shiraishi, A. Oya, *Electrochem. Solid-State Lett*. 5 (2002) A283.

[26] S. Yoon, J. Lee, T. Hyeon, S.M. Oh, *J. Electrochem. Soc.* 147 (2000) 2507.

[27] S. Jun, S.H. Joo, R. Ryoo, M. Kruk, M. Jaroniec, Z. Liu, T. Ohsuna, O. Terasaki, *J. Am. Chem. Soc*. 122 (2000) 10712.

[28] W. Xing, S.Z. Qiao, R.G. Ding, G.Q. Lu, Z.F. Yan, H.M. Cheng, *Carbon* 44 (2006) 216-224.

[29] H. Nishikara, T. Kyotani, *Adv. Mater.* 24 (2012) 4473.

[30] A. Sánchez-Sánchez, T.A. Centeno, F. Suárez-García, A. Martínez-Alonso, J.M.Tascón, *Microp. Mesop. Mater.* 235 (2016) 1.

[31] Y. Liu, J. Zhang, *Microp. Mesop. Mater.* 206 (2015) 81.

[32] J. Gao, X. Wang, Q. Zhao, Y. Zhang, J. Liu, *Electrochim. Acta* 163 (2015) 223.

[33] W. Yang, Y. Feng, D. Xiao, H. Yuan, *Int. J. Energy Res.* 39 (2015) 805.

[34] A. Jain, C. Xu, S. Jayaraman, R: Balasubramanian, J.Y. Lee, M.P. Srinivasan, *Microp. Mesop. Mater.* 218 (2015) 55.

[35] S. Tanaka, H. Fujimoto, J.F.M. Denayer, M. Miyamoto, Y. Oumi, Y. Miyake, *Microp. Mesop. Mater.* 217 (2015) 141.

[36] V. Meynen, P. Cool, E.F. Vasant, *Microp. Mesop. Mater.* 125 (2009) 170.

[37] T. Cottineau, M. Toupin, T. Delahaye, T. Brousse, D. Bélanger, *Appl. Phys. A* 82 (2006) 599-606.

[38]. E. Van Bavel, P. Cool, K. Aerts, E.F. Vansant, *J. Porous Mater.* 12 (2005) 65.

[39] F. Tuinstra, J.L. Koenig, J. Chem. Phys. 53 (1970) 1126-1130; L.M. Mard, M.A. Pimenta, G. Dresselhaus, M.S. Dresselhaus, *Physics Reports* 473 (2009) 51-87.

[40] Y. Gogotsi and V. Presser Eds., Carbon Nanomaterials 2nd Edition, CRC Press, Florida (2014), p. 112

[41] A. Sánchez-Sánchez, F. Suárez-García, A. Martínez-Alonso, J.M.D. Tascón, *Carbon* 70 (2014) 119-129.

[42] H. Mosqueda, O. Crosnier, L. Athouël, Y. Dandeville, Y. Scudeller, Ph. Guillemet, D.M. Schleich, T. Brousse, *Electrochim. Acta* 55(25) (2010) 7479-7483.

[43] J. Lee, J. Kim, Y. Lee, S. Yoon, S.M. Oh, T. Hyeon, *Chem. Mater.* 16 (2004) 3323.

Figure 1
Click here to download high resolution image

FIGURE 1

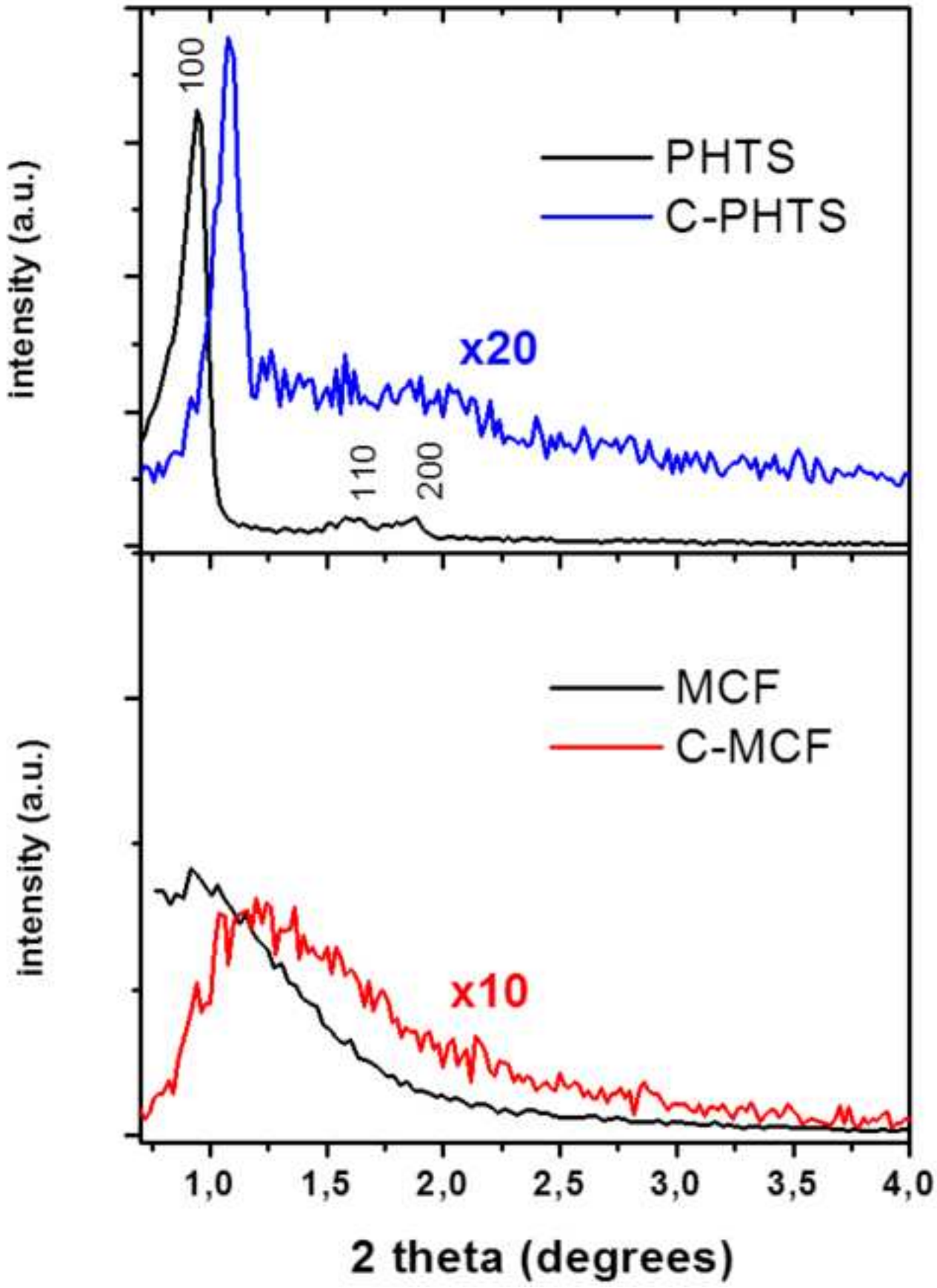

Figure 2
Click here to download high resolution image

FIGURE 2

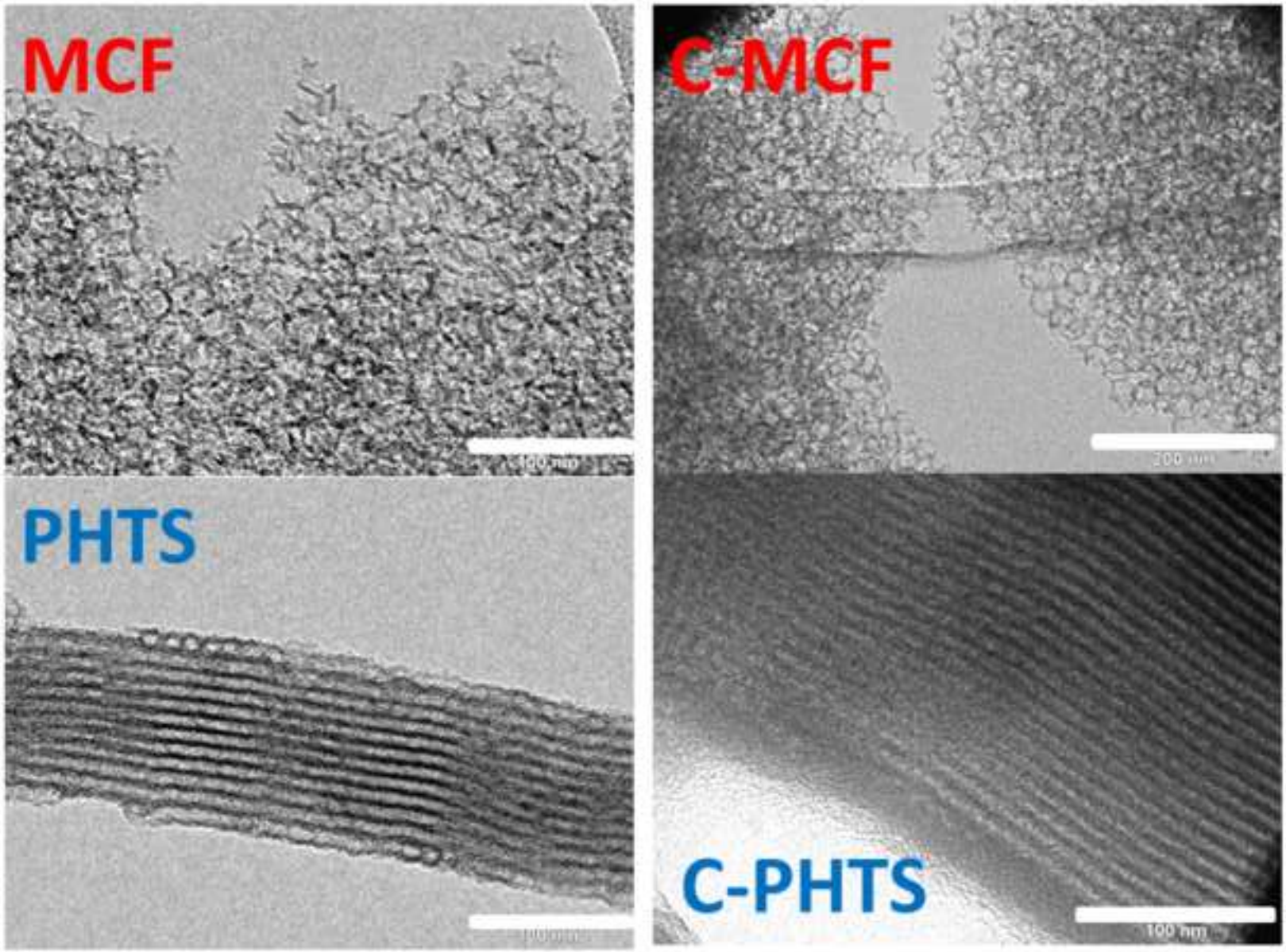

Figure 3
Click here to download high resolution image

FIGURE 3

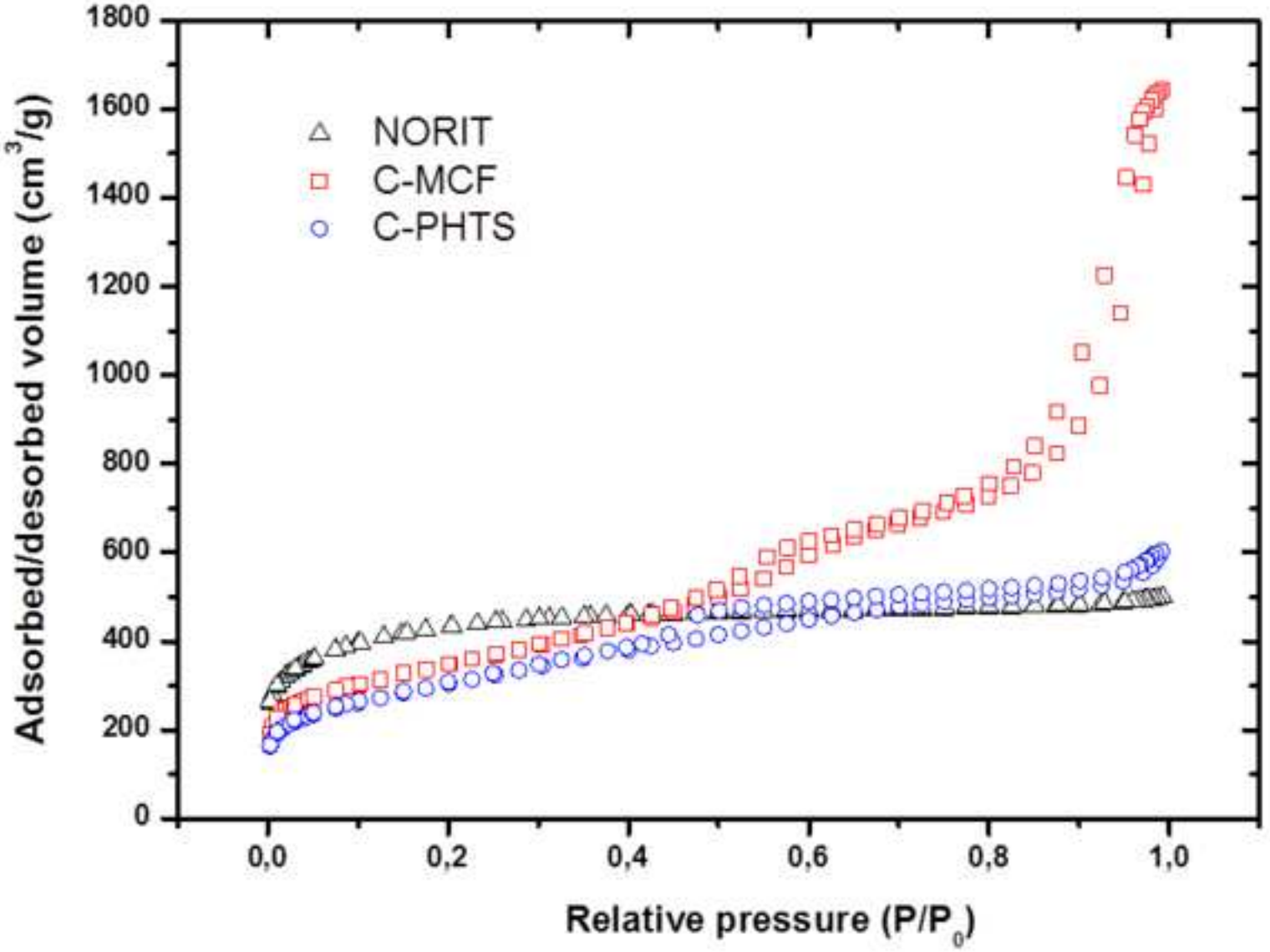

Figure 4

Click here to download high resolution image

FIGURE 4

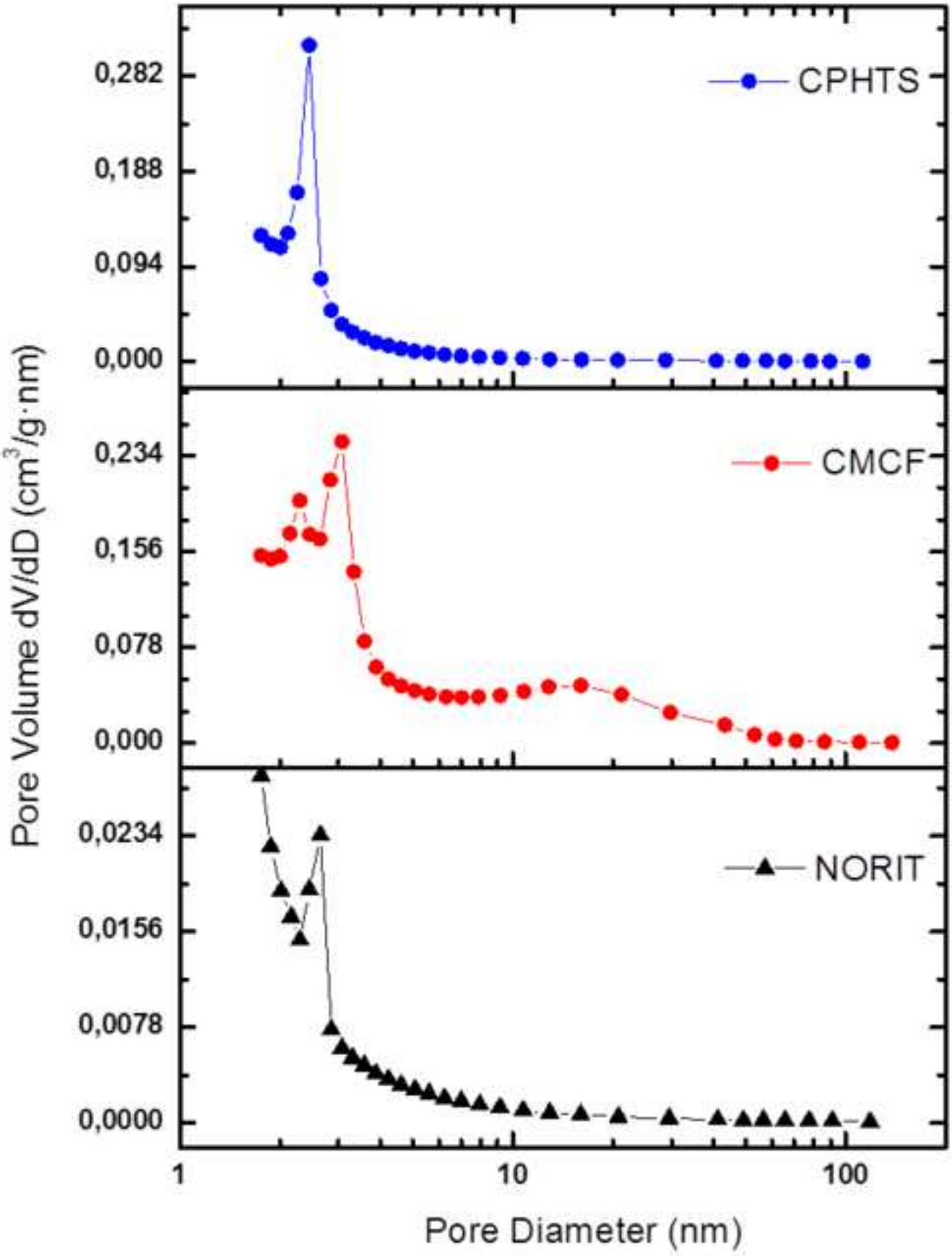

Figure 5
Click here to download high resolution image

FIGURE 5

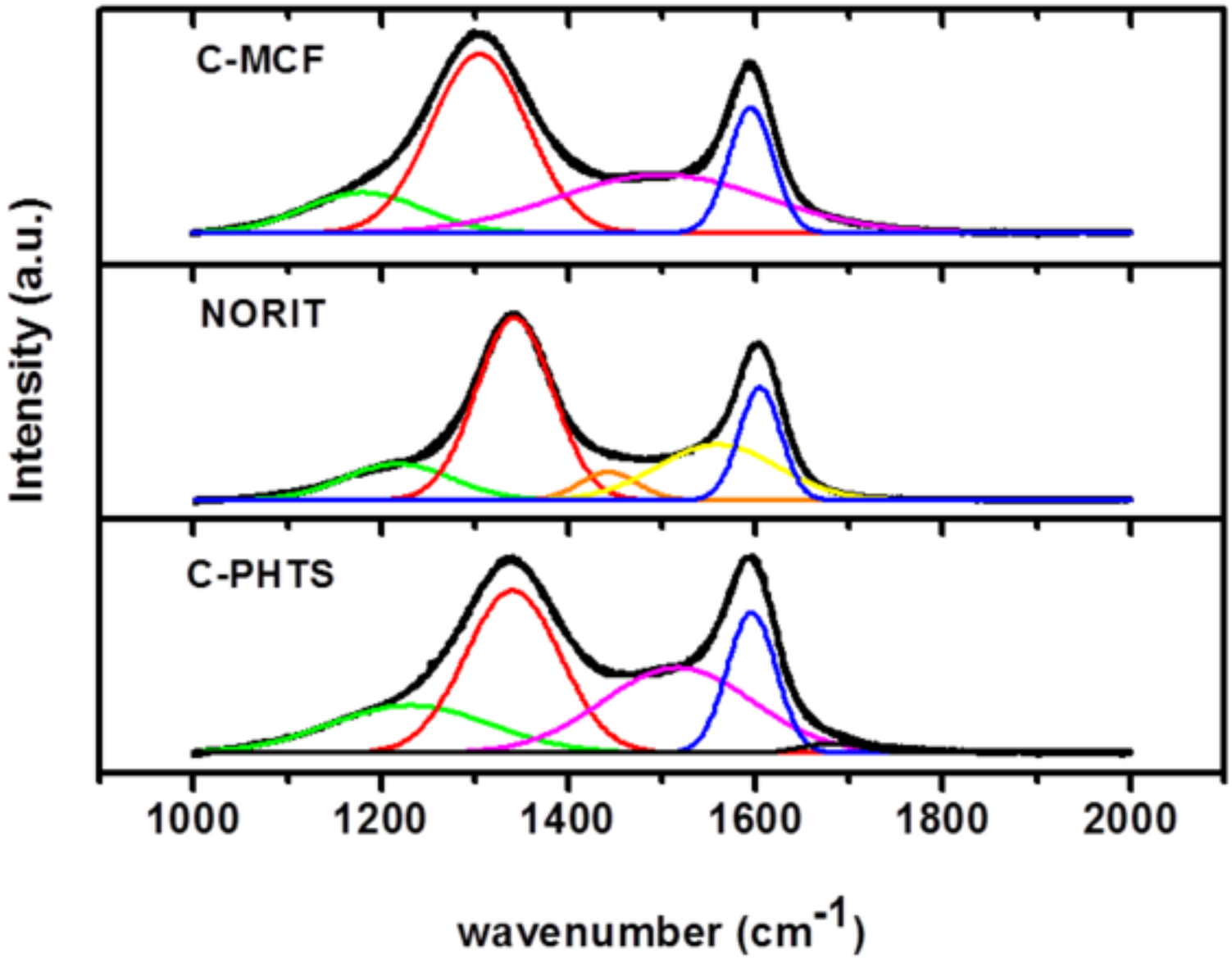

Figure 6
Click here to download high resolution image

FIGURE 6

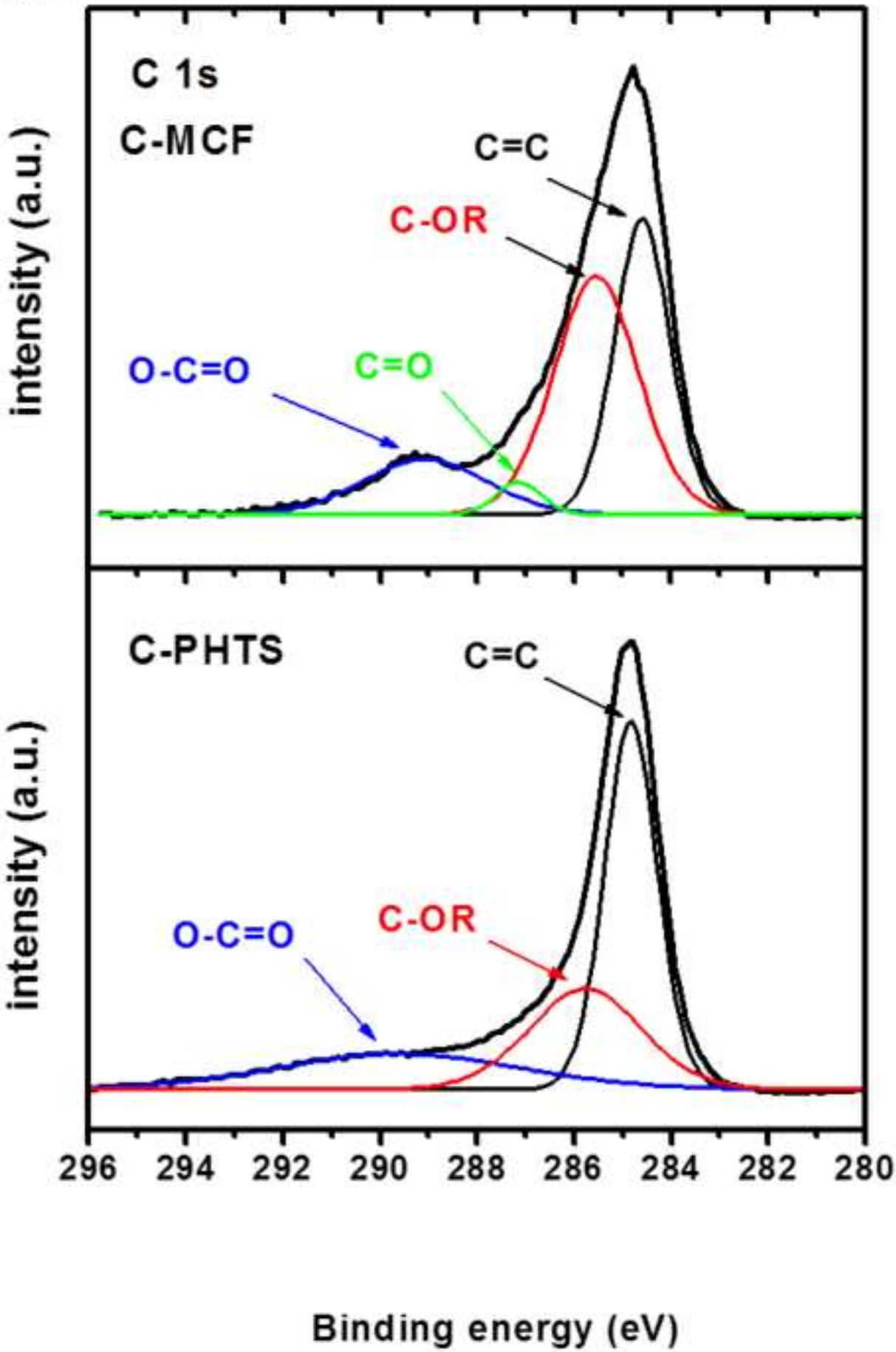

Figure 7
Click here to download high resolution image

FIGURE 7

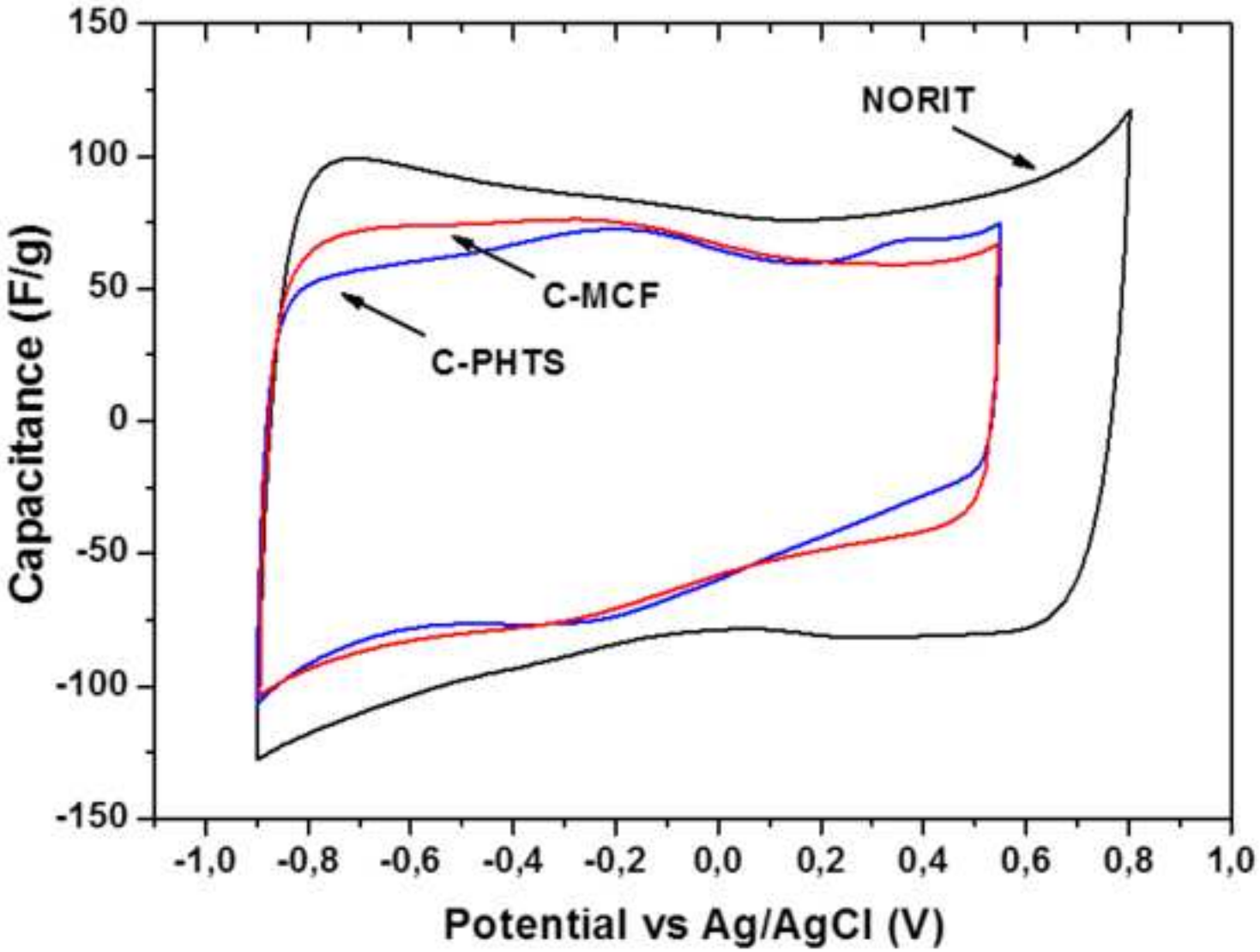

Figure 8
Click here to download high resolution image

FIGURE 8

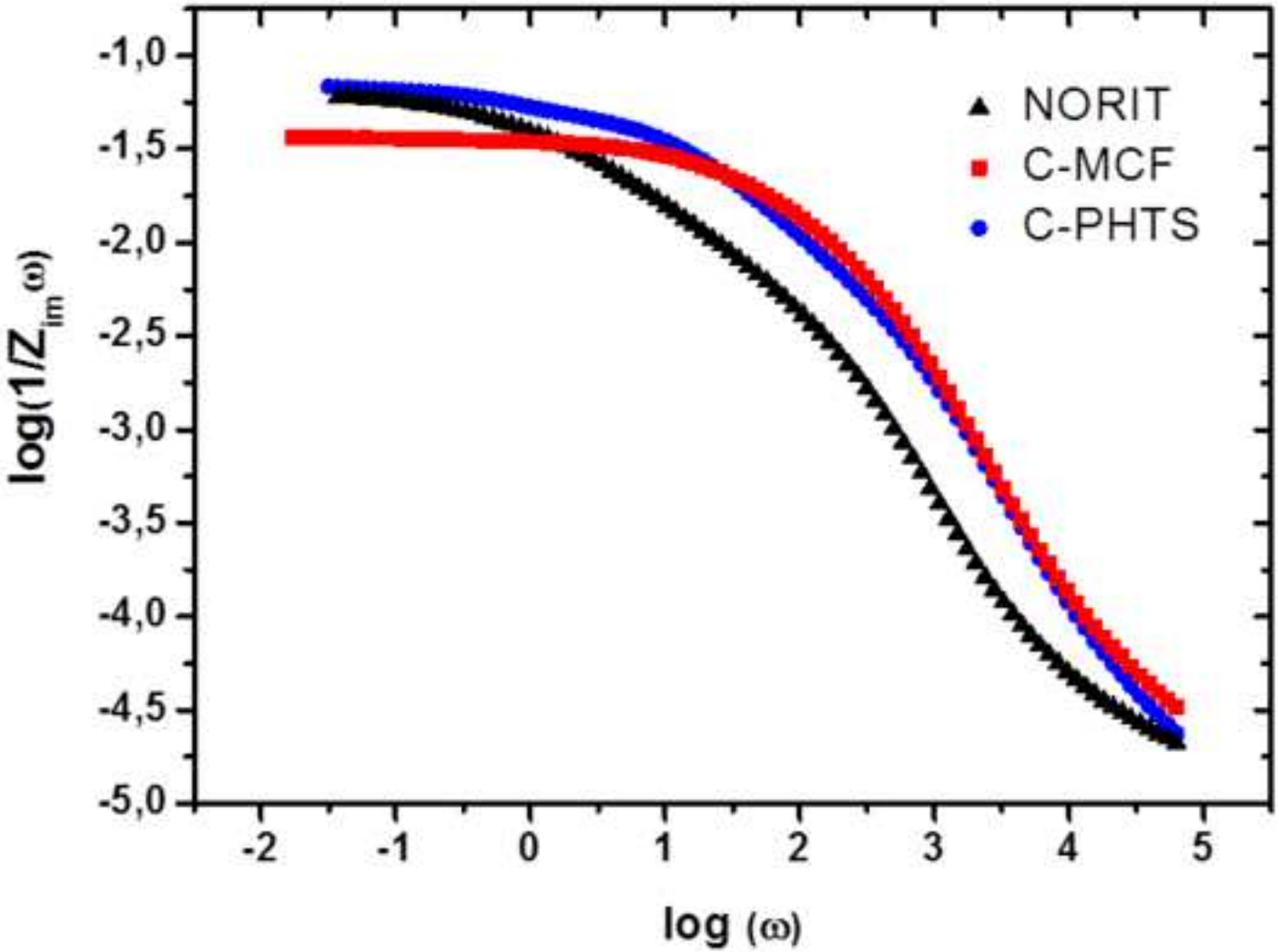

Figure 9
Click here to download high resolution image

FIGURE 9

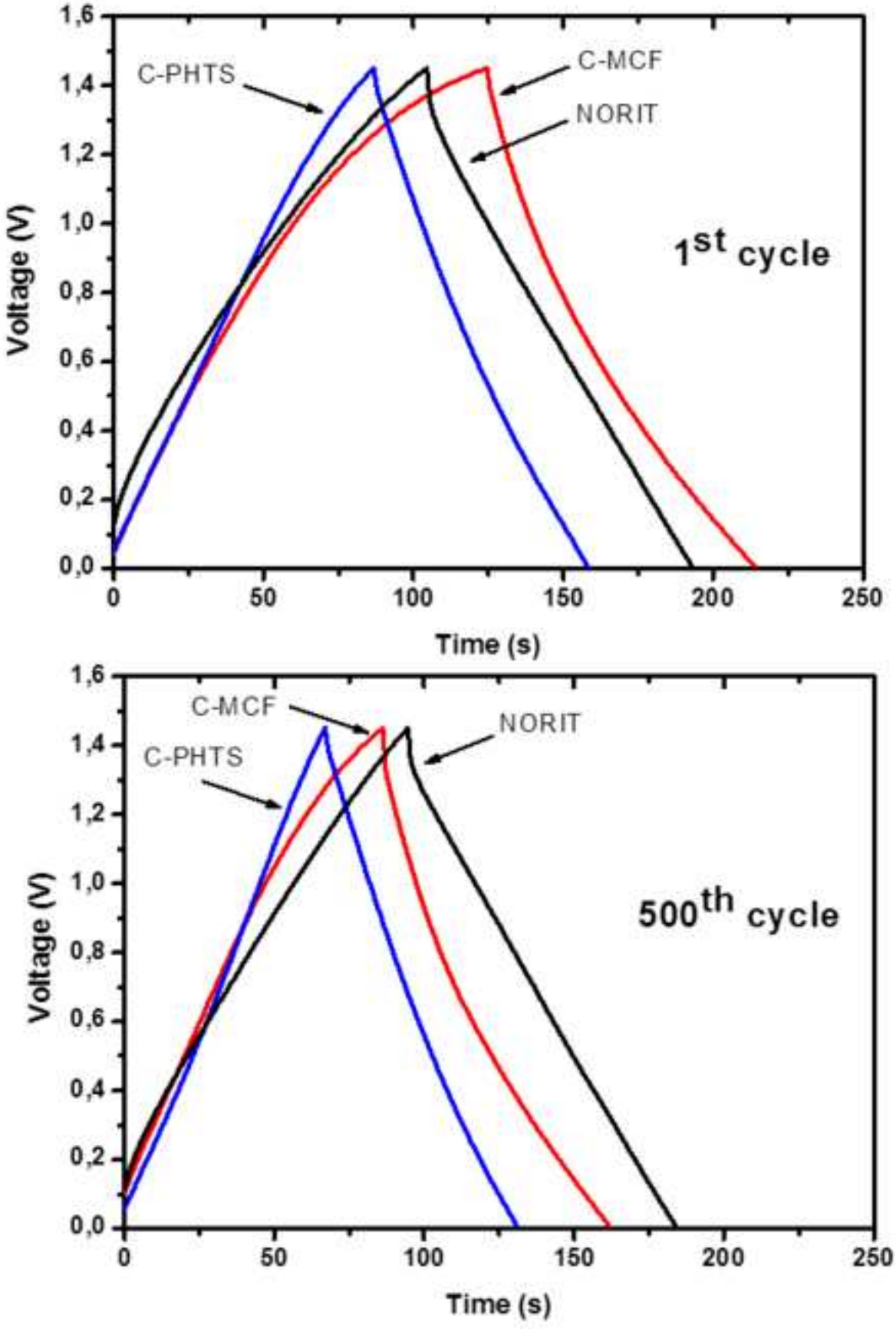

Figure 10

Click here to download high resolution image

FIGURE 10

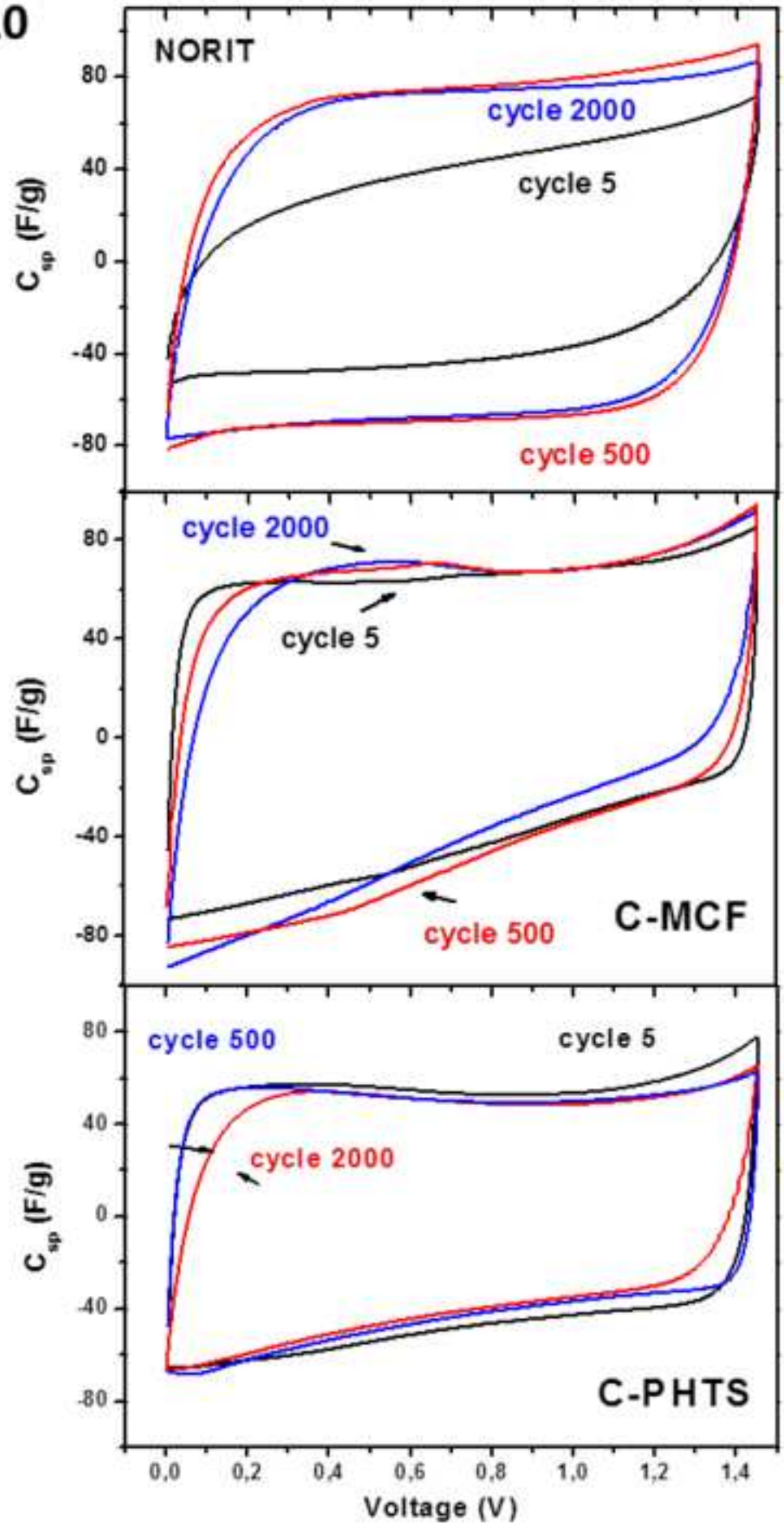

Figure 11
Click here to download high resolution image

FIGURE 11

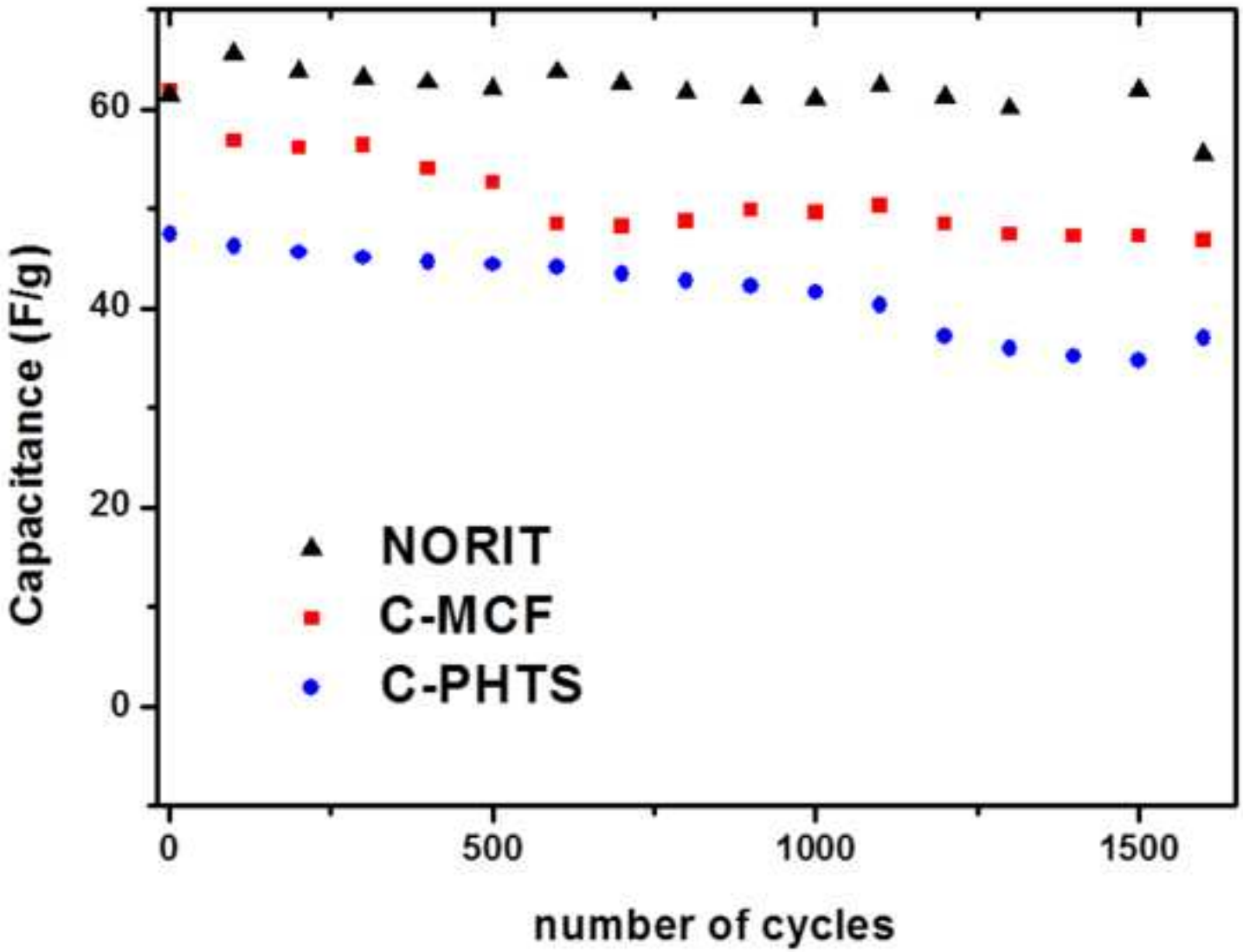

Figure 12
Click here to download high resolution image

FIGURE 12

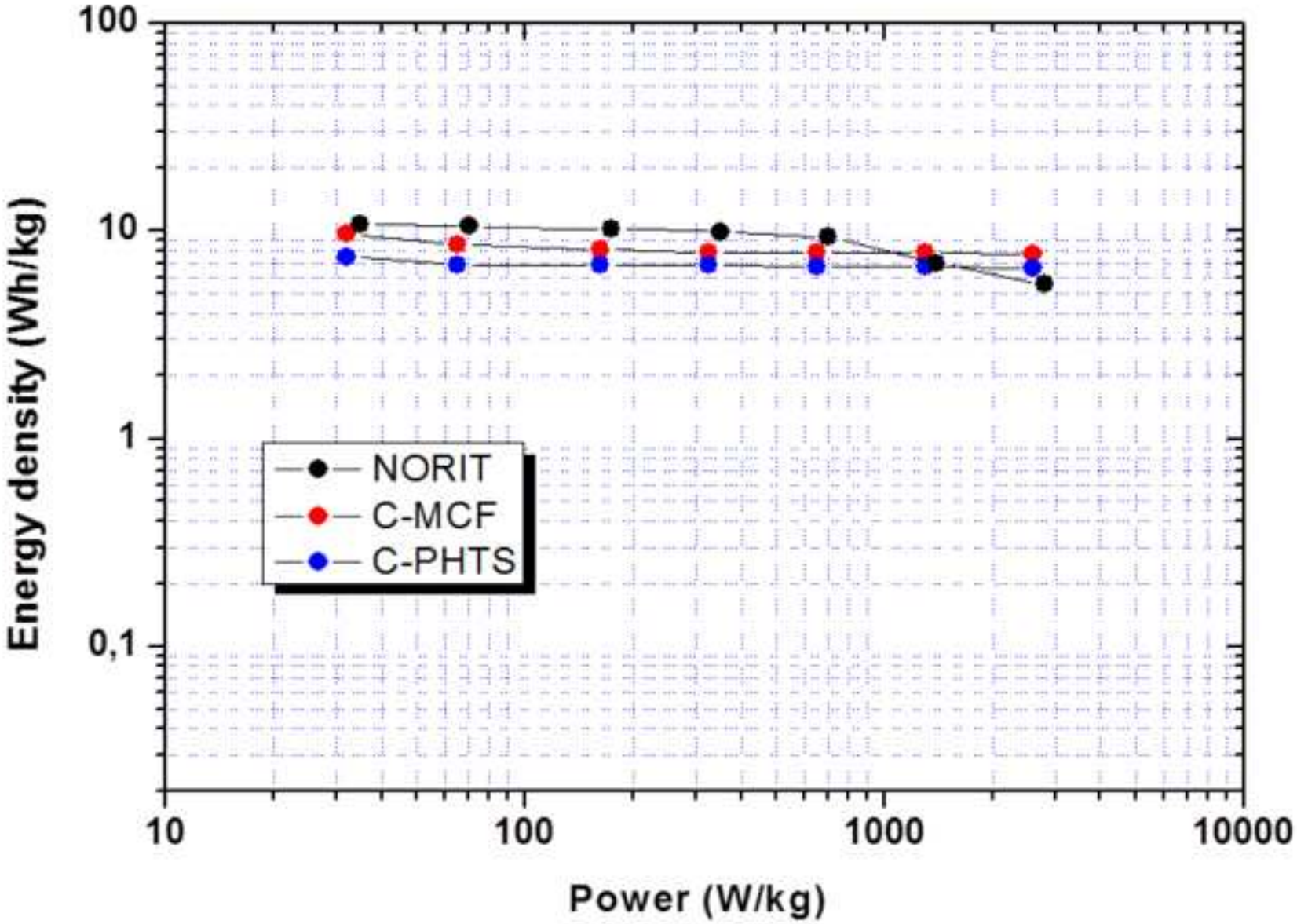

Figure 13
Click here to download high resolution image

FIGURE 13

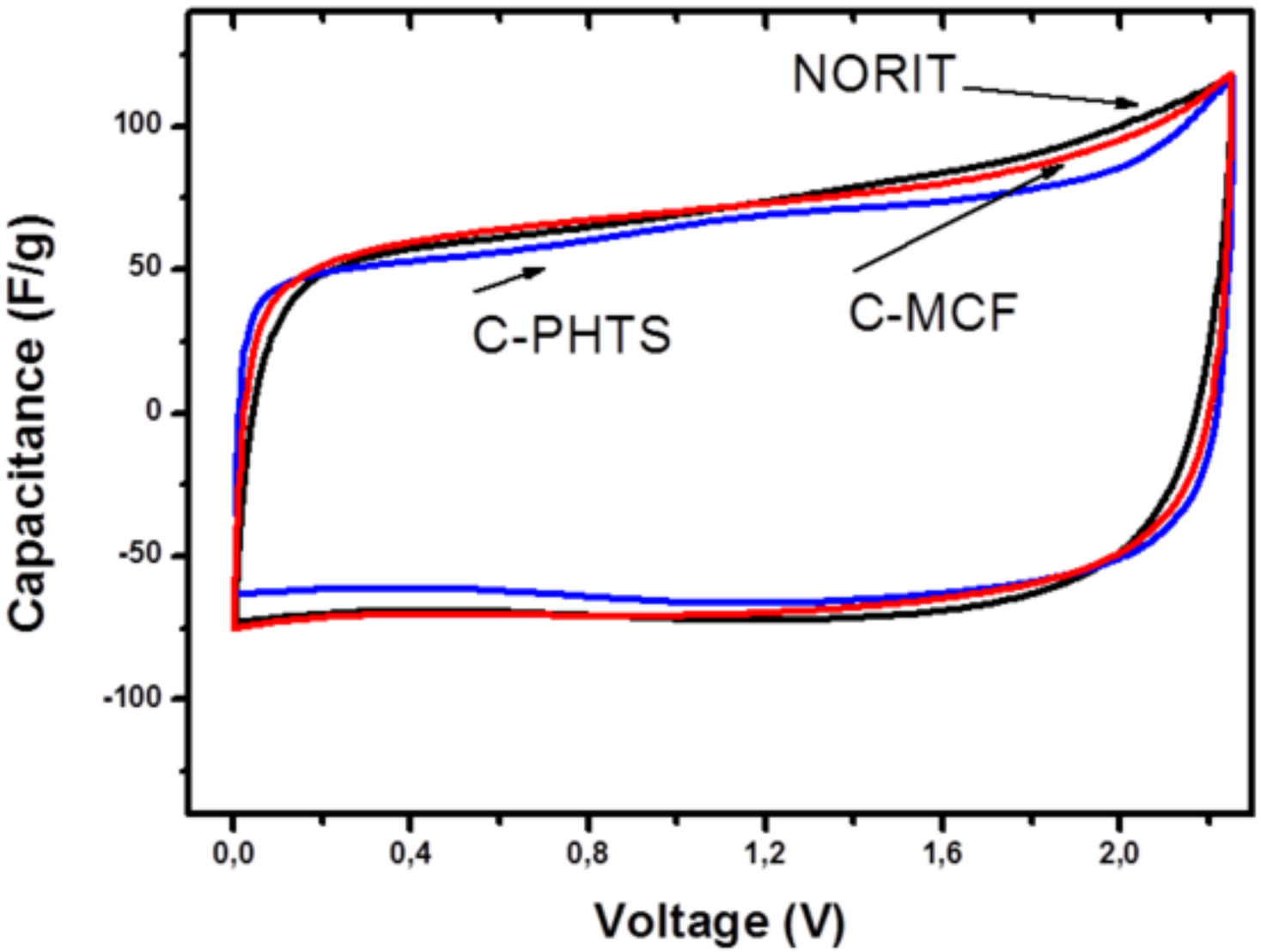

Table 1. Physicochemical parameters of the carbons studied in this work.

Sample	S_{BET} ($m^2 \cdot g^{-1}$)	V_{pore} ($cm^3 \cdot g^{-1}$)	$V_{micropore}$ ($cm^3 \cdot g^{-1}$)	$<d_{pore}>$ (nm)	D/G
NORIT	1400	0.77	0.39	2.2	3.00
C-MCF	1215	2.54	0.10	8.1	3.06
C-PHTS	1050	0.93	0.07	3.2	2.24

Table 2

Table 2. Energetic parameters of the supercapacitor symmetric devices studied in this work.

	1st cycle			500th cycle		
Electrode	Capacitance ($F \cdot g^{-1}$)	ESR (Ω)	E_{real} ($Wh \cdot kg^{-1}$)	Capacitance ($F \cdot g^{-1}$)	E_{real} ($Wh \cdot kg^{-1}$)	P_{max} ($kW \cdot kg^{-1}$)
NORIT	61	17.4	8.9	62	8.9	26
C-MCF	62	7.5	9.0	52	7.7	64
C-PHTS	47	9.0	7.3	44	6.5	53

Table 3

Table 3. Energetic densities of supercapacitor devices working in aqueous electrolytes. *Data obtained in a three electrodes configuration with [1]Ag/AgCl or [2]Hg/HgO reference electrode.

					Energy (Wh/Kg)			
Electrode	Electrolyte	Voltage limits (V)	Activation agent	Capacitance* ($F \cdot g^{-1}$)	Low P	Middle P	High P	Ref
NORIT	0.5M Na_2SO_4	0;1.45 V	Yes	80*[1] (20 mVs^{-1})	10.5 (70 Wkg^{-1})	9.3 (0.7 $kWkg^{-1}$)	5.5 (2.8 Wkg^{-1})	This work
C-MCF	0.5M Na_2SO_4	0;1.45V	Not	75*[1] (20 mVs^{-1})	8.6 (65 Wkg^{-1})	7.8 (0.65 $kWkg^{-1}$)	7.7 (2.6 Wkg^{-1})	This work
C-PHTS	0.5M Na_2SO_4	0;1.45V	Not	65*[1] (20 mVs^{-1})	6.8 (65 Wkg^{-1})	6.7 (0.65 $kWkg^{-1}$)	6.6 (2.6Wkg^{-1})	This work
Maxsorb	30% w. KOH	-0.9V;0V	KOH	178*[1] (20 mVs^{-1})	9.4 (0.2 $kWkg^{-1}$)	4.2 (0.32 $kWkg^{-1}$)	2.3 (0.4 $kWkg^{-1}$)	Lu et al. [28]
Maxsorb	1M H_2SO_4	-0.2V;0.6V	KOH	178*[1] (1 mVs^{-1})	19*[1] (65 Wkg^{-1})	18*[1] (0.65 $kWkg^{-1}$)	16*[1] (2.5 $kWkg^{-1}$)	Tanaka et al.[35]
Maxsorb	1M H_2SO_4	-0.2V;0.6V	HNO_3	232*[1] (1 mVs^{-1})	28*[1] (65 Wkg^{-1})	18*[1] (0.65 $kWkg^{-1}$)	9*[1] (2.5 $kWkg^{-1}$)	Tanaka et al.[35]
OMC (MCM-48)	30% w. KOH	-0.9V;0V	Not	193*[1] (20 mVs^{-1})	6 (0.1 $kWkg^{-1}$)	5 (0.6 $kWkg^{-1}$)	4 (0.8 $kWkg^{-1}$)	Lu et al. [28]
OMC (SBA-15)	30% w. KOH	-0.9V;0V	Not	191*[1] (20 mVs^{-1})	5.9 (0.1 $kWkg^{-1}$)	5.2 (0.6 $kWkg^{-1}$)	5.1 (1.05 $kWkg^{-1}$)	Lu et al. [28]
OMC (KIT-6)	6M KOH	-1V,0V	Not	189[2] (20 mVs^{-1})	n.a.	7.0*[2] (1.4 $kWkg^{-1}$)	6.8*[2] (2.6 $kWkg^{-1}$)	Gao et al. [32]
OMC	1M H_2SO_4	-0.2V;0.6V	KOH	237*[1] (1 mVs^{-1})	16*[1] (65 Wkg^{-1})	12*[1] (0.6 $kWkg^{-1}$)	10*[1] (2.5 $kWkg^{-1}$)	Tanaka et al.[35]
OMC	1M H_2SO_4	-0.2V;0.6V	HNO_3	283*[1] (1 mVs^{-1})	22*[1] (65 Wkg^{-1})	20*[1] (0.6 $kWkg^{-1}$)	20*[1] (2.5 $kWkg^{-1}$)	Tanaka et al.[35]
AC from biomass	0.5M H_2SO_4	0;1 V	$ZnCl_2$	230 (0.5A/g)	8.7 (0.75 Wkg^{-1})	8.0 (1.4 $kWkg^{-1}$)	7.6 (2.3Wkg^{-1})	Srinivasan et al. [34]